

Type 2 Actuator Final Report

For:
NASA Langley Research Center
Hampton, Virginia

Under Contract No. NAS1-98035

By
Alson E. Hatheway Inc.

787 West Woodbury Road, Unit # 10
Altadena, California 91001

AEH Document No. 93607
Rev. A, 30 August 1999

Table of Contents

	Page
1.0 Introduction	2
2.0 Test Facilities	2
2.1 JPL's Cryogenic Temperature Test Facility	3
2.2 SMD's Room Temperature Test Facility	4
3.0 The Test Program at JPL	5
3.1 The Influences of Temperature on the Actuator's Performance	5
3.2 The Positions of the Hard-Stops	5
3.3 Testing the Strokes of the Coarse and Fine Stages	6
3.4 Testing the Smallest Increment of the Coarse Stage	6
3.5 Testing the Smallest Increment of the Fine Stage	7
3.6 Testing Cryogenic Heat Dissipation	9
3.7 Discussion of the Test Data from JPL	10
4.0 The Test Program at Moog-SMD	12
4.1 Testing the Smallest Increment of the Fine Stage	13
4.2 Testing Room Temperature Power Consumption	13
4.3 Testing the Mass of the Actuator	14
4.4 Discussion of the Test Data from Moog-SMD	14
5.0 Analysis of the Other Properties	15
5.1 Analysis of the Elastic Properties of the Fine Transducer	15
5.2 Analysis of Creep	15
5.3 Analysis of Loads Between the Lead Screws and Nuts	16
5.4 Analysis of Lifecycles	16
5.5 Analysis of the Motor Size	17
5.6 Analysis of the Axial Stiffness	17
5.7 Analysis of Axial Force, Set & Hold	18
5.8 Analysis of Thermal Stability	18
6.0 An Analytical Model of Actuator for System Simulations	18
7.0 Requirements Compliance Matrix	19
8.0 Installation Data	19
9.0 References	19

Appendices

A. Thermal Stability	20
B. Interface Control Drawing	21

1.0 Introduction

A two-stage Rubicon™ actuator, a sectional view of which is shown in Figure 1, has been jointly developed by Alson E. Hatheway Inc. (AEH) and the Schaeffer Magnetics Division of Moog Inc. (SMD) for use on the Next Generation Space Telescope Project (NGST) under a prime contract to NASA's Langley Research Center, Hampton, Virginia.

AEH and SMD have completed a program to evaluate the characteristics of the Rubicon dual-stage actuator at both room temperature and cryogenic temperature. Two different test facilities were used for tests: a cryogenic test facility at Cal Tech's Jet Propulsion Laboratory (JPL) in Pasadena, California, and a room temperature facility specially set up for this project at SMD in Chatsworth, California. Only room temperature measurements were made at SMD while both room temperature and cryogenic temperature measurements were made at JPL. The results of these tests are presented and discussed in the following sections of this report.

Some properties of the actuator have been evaluated analytically. These are discussed in section 5.0.

The prime mover for the actuator is a high reliability space-rated stepper motor designed and constructed by SMD. The stepper motor produces twenty-four full steps per revolution. Micro-stepping is not used in the Rubicon which allows it to hold position with the power off. The stepper motor drives a lead-screw through a reducing gearbox with a ratio of about 1/45.2, producing about 1085 motor steps per revolution of the lead screw. The lead screw uses a 40-pitch thread form (.025 inches, .635 millimeters, of lead). The basic resolution of this combination is .585 micrometers of axial motion for each motor step. The coarse stage of the two-stage Rubicon actuator uses sixteen full turns of its lead screw to produce more than ten millimeters of stroke in increments of .585 micrometers. In the coarse stage the lead screw mechanism is "inverted" so that the nut turns and the screw translates axially.

The same motor, gear box and lead screw (not "inverted") combination is used in the fine stage but the output motion is reduced by a factor of .00462 in the Rubicon transducer (Figure 2). The fine stage is designed to produce a nominal axial motion of about 3.0 nanometers for each step in the fine motor. Ten turns of the fine lead screw are used to produce a total stroke greater than about 30 micrometers in the fine stage.

The output of both the fine and the coarse stages are summed at the actuator's output shaft. This permits both coarse adjustment activities and fine alignment activities to be performed with the same actuator.

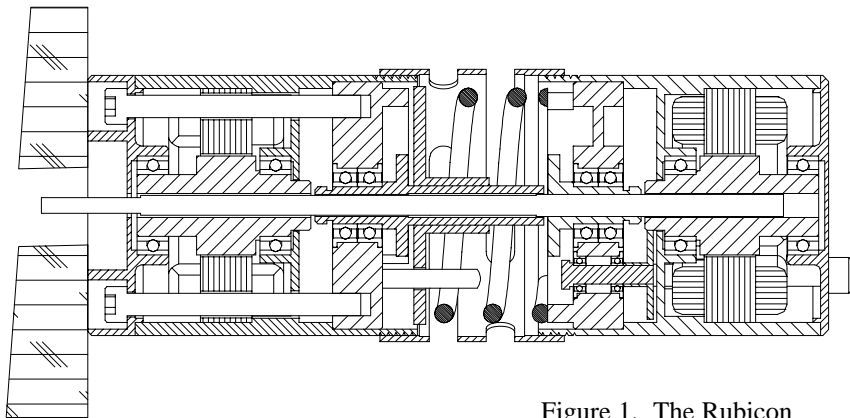


Figure 1. The Rubicon cryogenic actuator in sectional view

2.0 Test Facilities

2.1 JPL's Cryogenic Temperature Test Facility

JPL's cryogenic test facility consists of a vertical stainless steel dewar and a vertical stainless steel test bench. The test bench is designed to be lifted by overhead crane and dropped vertically into the dewar. The test bench has a stainless steel bulkhead which comes to rest on the top rim of the dewar and an 'O' ring effects a vacuum seal for the contents and everything mounted on the test bench. Four services are provided through



Figure 2. The Rubicon transducer

the bulkhead: electrical services for operation of the test article, electrical connections for monitoring temperatures in the test space, a cryogen supply to keep the test article at the desired temperature and an optical window which permits the measurement leg of an interferometer to measure the output position of the test article.

Figure 3 shows the test bench outside the dewar and resting in a pipe fixture. At the bottom can be seen the cryogen vessel. The facility uses both liquid nitrogen (77° K) and liquid helium (5° K) as cryogens. On top of the cryogen vessel is the fixture supporting the Rubicon actuator (see Figure 4). At the top of the bench can be seen the bracket that supports the Polytech Series 3000 Vibrometer (interferometer) head so its measurement leg is directed through the optical window and down the geometric center to the output rod of the actuator. The Polytech's bracket is attached to the top side of the bulkhead which will seal the dewar when the test bench is lowered into it. Between the bulkhead and the actuator/cryogen vessel may be seen three three-quarter inch diameter rods which control the position of the test article with respect to the Polytech interferometer. One may also see three foil disks (horizontal) which act as thermal radiation shields between the cryogen vessel/actuator and the bulkhead, a potentially large heat leak into the cold section of the installation.

The Polytech Series 3000 instrument operates at a wavelength of about 630 nanometers and has a resolution limit of about 1% of the wave length, 7 nanometers. It is capable of very high rates of data collection (kilohertz) and can be used to observe dynamic behavior (therefore its description as a vibrometer by the manufacturer). The data are recorded on a computer workstation and a typical data file contains over 16,000 measurements. The workstation that collects the data also has graphics software for observing and analyzing the data. For detailed analysis the data files were converted to ASCII text files and read into a commercial spreadsheet program (Microsoft Excel). The charts presented here that are based upon the JPL test data were prepared in this software.

2.2 SMD's Room Temperature Facility

The SMD testing facility uses precision capacitance gauging metrology techniques developed by AEH for characterizing their precision actuators (Hatheway, 1994). The technique uses an air-gap capacitor as the sensing element. The area of the capacitor plates is about half a square inch and with air gaps of 200 to 300 micrometers the capacitance is between 10 and 15 picofarads. One capacitor plate is attached to the end of the actuator's thrust rod and the other is held rigidly fixed. The actuator, capacitance plates and related fixtures are supported on a granite surface plate for stability. The facility may be seen in Figure 5. The granite surface plate, actuator, capacitor plates and fixtures may be seen centered in the back of the figure.

The capacitance is measured with an Andeen-Hagerling 2500A/E precision capacitance bridge (in the lower foreground of Figure 5) which can measure the capacitance to eight significant figures. A change of one unit in the sixth figure represents about 2 nanometers.

The capacitance data are recorded on a lap top computer (partly visible in the right side of Figure 5). The data are transferred to another computer for both viewing and analysis in a spreadsheet program (both Microsoft Excel and Lotus 1-2-3 are employed). All the charts presented here that are based upon SMD data were prepared in Microsoft Excel.

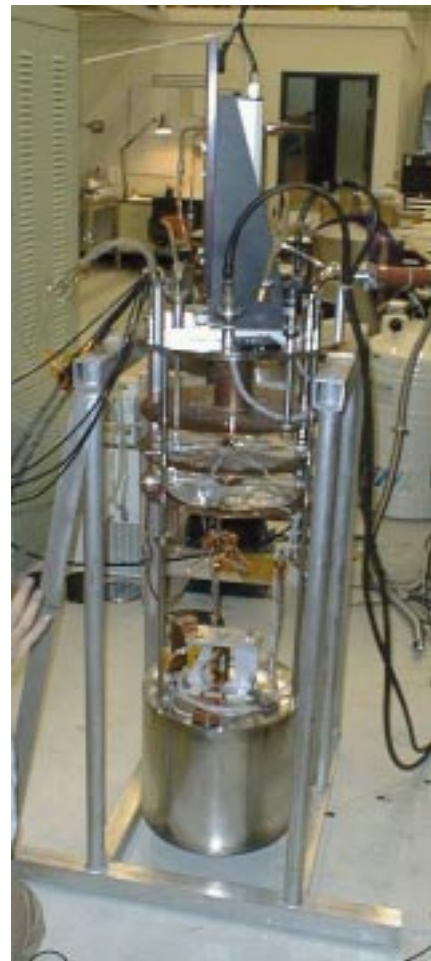


Figure 3. The test bench of JPL's cryogenic test facility.

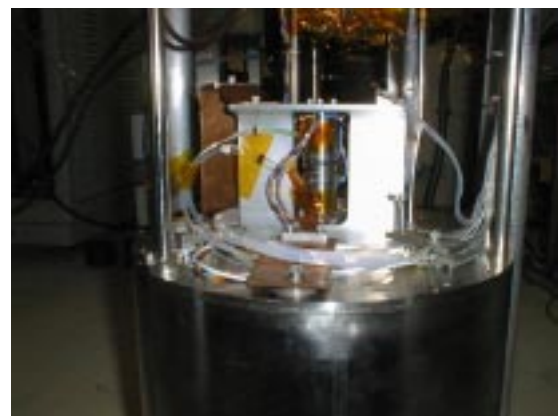


Figure 4. Detail of the Rubicon installed at JPL.

3.0 The Test Program at JPL

The program began with installation of the Rubicon actuator in the test bench at JPL, a visual inspection and electrical check followed by installation in the dewar. Before the dewar was sealed the actuator was exercised to be sure that everything was working well.

After the successful exercise the dewar was sealed, evacuated and then chilled; first with liquid nitrogen then with liquid helium. The vacuum was maintained at about 100 millitorr. After about 24 hours the temperatures stabilized at about 20° K for the fine stage motor and about 30° K for the coarse stage motor (the coarse stage motor was farther from the cryogen than the fine stage motor). The actuator was exercised to verify

survival at cryogenic temperatures and then the behavior of the actuator was studied in considerable detail at the low temperature and the data recorded. The data included coarse stage stroke capacity and smallest increment as well as fine stage stroke capacity and smallest increment. The data from the measurement of the smallest increments of the fine stage were difficult to repeat accurately. It was difficult to determine the cause of the lack of repeatability; external environmental factors, limited resolution of the interferometer, unpredictable defects in the actuator or parasitic motor effects such as motor and frictional heating may each contribute.

The test article was allowed to warm somewhat and stabilize at about 80° K which is a normal thermal plateau on the way back to room temperature. More data were collected at this temperature and the behavior was observed to be indistinguishable from that at the cryogenic temperature including the influences generating uncertainty and poor repeatability in the smaller measurements.

The test article was then allowed to return to room temperature, a process that takes several days. A detailed study of the behavior at room temperature was made and data collected. The data appeared again to be indistinguishable from the cryogenic data including the uncertainty and poor repeatability of the smaller measurements.

3.1 The Influences of Temperature on the Actuator's Performance

The Rubicon actuator was designed specifically so its performance characteristics would be independent of temperatures over the range from 20° K to 300° K. Within the accuracy and stability of the instruments used in this test program this goal has been achieved. Both room temperature and cryogenic temperature data are presented here, interchangeably, and truly either is representative of both in terms of the actuator's performance.

3.2 The Position of the Hard-Stops

We first established the positions for the hard-stops that determine the limits of motion for the coarse and fine stages. A stage was driven through short distances in one direction until the indicated motion (from the Polytech 3000) was observed to fall off or stop. The direction was reversed and small steps repeated to determine the location at which the actuator was free of the stop. The actuator was then driven to the opposite hard stop which was approached in small steps. When the stop was encountered the actuator was reversed and the point determined at which it came free of the stop. By this method

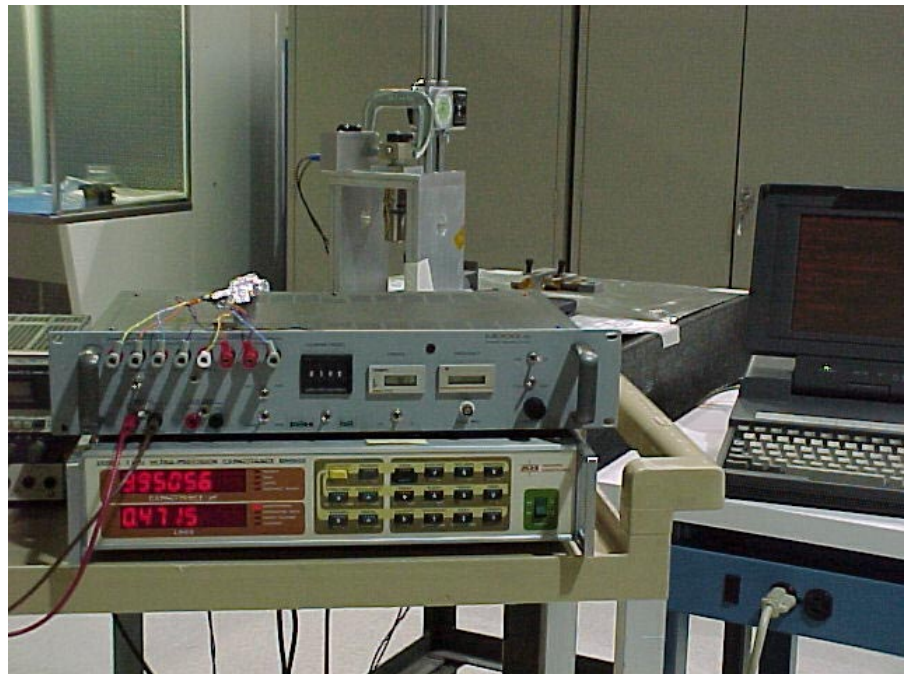


Figure 5. The Rubicon installed in SMD's Room Temperature Test Facility

the number of clear motor steps between the hard-stops for both the fine and coarse stages was determined:

Coarse:	17,680 motor steps = 10.33 millimeters
Fine:	9,836 motor steps = 31.94 micrometers.

The positions of the hard-stops were determined at cryogenic temperature. During subsequent operations logs were maintained for both the coarse and fine stages to avoid hitting the hard-stops. Since some of the output motions of the actuator are very small it may take many motor steps to become aware that a stop has been encountered. During an encounter with a hard stop the motion of the actuator is influenced by the stop, creating spurious output motions. It was decided to continuously track the positions of both stages (coarse and fine) using operating logs to avoid contact with the stops during testing. Each of the stages was generally maintained in its mid-stroke position when it was not the subject of a particular test. Likewise, at the end of a test of one of the stages it was returned to its mid-stroke position.

3.3 Testing the Strokes of the Coarse and Fine Stages

After determining the position of the hard stops both stages were positioned in mid-stroke. The coarse stage was operated over a range of ± 8670 motor steps. It was performed in four parts; first extending it in one burst of 8670 motor steps, then retracting it in one burst of 8670 motor steps, then retracting it again in one burst of 8670 motor steps each and finally extending it in one burst of 8670 motor steps (returning it to its mid-stroke position). This range of motion was selected to demonstrate the actuator's stroke as greater than 10 millimeters while avoiding hitting the hard stops. Figure 6 shows the resulting data taken at room temperature.

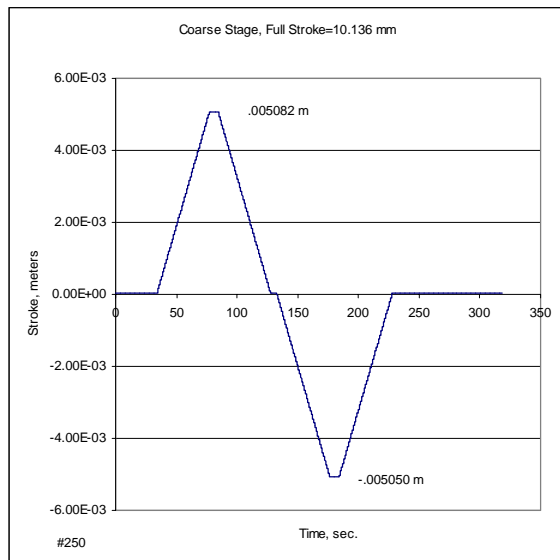


Figure 6. Stroke of coarse stage.

The fine stage was then operated over its stroke twice. It was first positioned near the hard stop in the retracted position. It was then extended in eight bursts of 1000 motor steps each, retracted in eight bursts of 1000 motor steps each and finally these two operations were repeated (returning it to a position near the retracting hard stop). As with the coarse stage, this range was selected to demonstrate the stroke of the fine stage while avoiding its hard stops. The resulting room temperature data are shown in Figure 7.

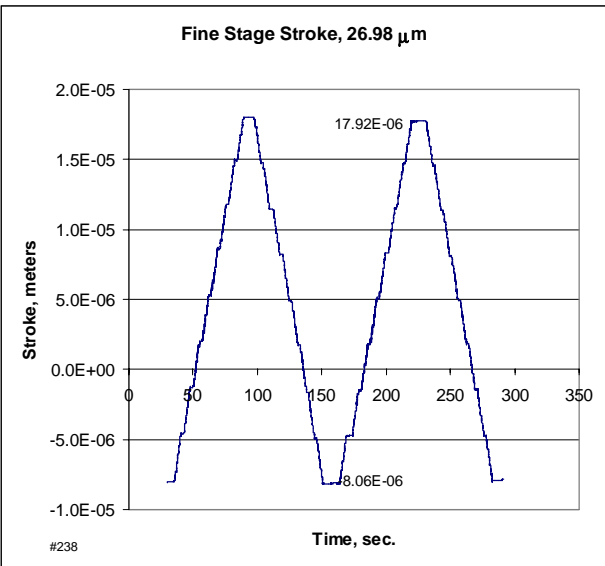


Figure 7. Stoke of fine stage.

3.4 Testing the Smallest Increment of the Coarse Stage

The smallest increment of motion of the coarse stage was demonstrated by running ten single steps followed by a burst of 100 motor steps, all retracting. The data are shown in Figure 8 and a detail of one of the steps is shown in Figure 9. Analysis of the data shows that the smallest increment of motion is a single motor step. Its average size is .58 micrometers

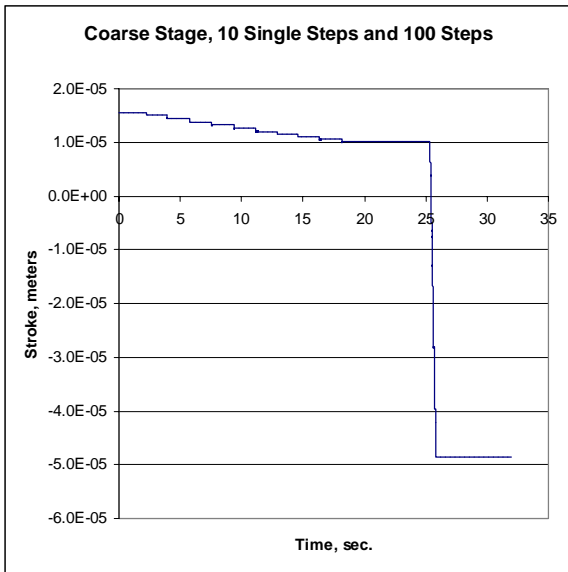


Figure 8. Coarse stage increments

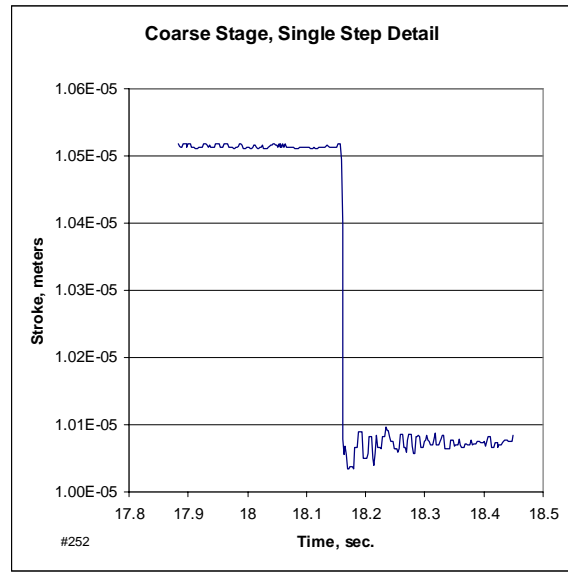


Figure 9. Detail of a coarse increment

and they have a variability of .074 micrometers, rms. These data were taken in the JPL facility in vacuum at room temperature. Data taken at cryogenic temperature are indistinguishable from these. The smallest increment of the coarse stage is equal to its resolution, one step of the motor.

3.5 Testing the Smallest Increment of the Fine Stage

The smallest increment of the fine stage was demonstrated by a similar sequence of motor steps: ten identical bursts of a few (between one and ten) motor steps followed by one burst of 100 motor steps for reference.

3.5.1 Response to Ten Bursts of Ten Motor Steps Followed by One Burst of 100 Motor Steps

Figure 10 shows the response of the actuator (at JPL) to ten bursts of ten steps followed by a burst of 100 steps (retracting) at room temperature. The burst of 100 steps may be used as a benchmark to determine the displacement associated with a single motor step. The 100 motor step burst caused a motion of about 325 nanometers and one motor step would be equivalent to 3.25 nanometers (the resolution of the fine stage). Applying this value to the ten bursts of ten motor steps suggests that each burst of ten motor steps should move the fine stage by 32.5 nanometers. The train of ten such bursts should cause a net motion of 325 nanometers. In Figure 10 the train of ten bursts caused an apparent net motion of about 350 nanometers. To understand why this apparent motion is larger than 100 motor steps input in a single burst notice that in Figure 10 the data after about 28 seconds is a quiescent period in which we can observe a slight drift downward. In a twenty-second period (the time taken for the ten bursts of ten motor steps each) the drift amounts to between 20 and 30 nanometers in this quiescent period. If we remove the influence of this drift from the data for the ten bursts of ten motor steps (100 motor steps total) their net motion effect agrees quite well with the 100 motor steps taken as a single burst. It is then clear that the resolution of the fine

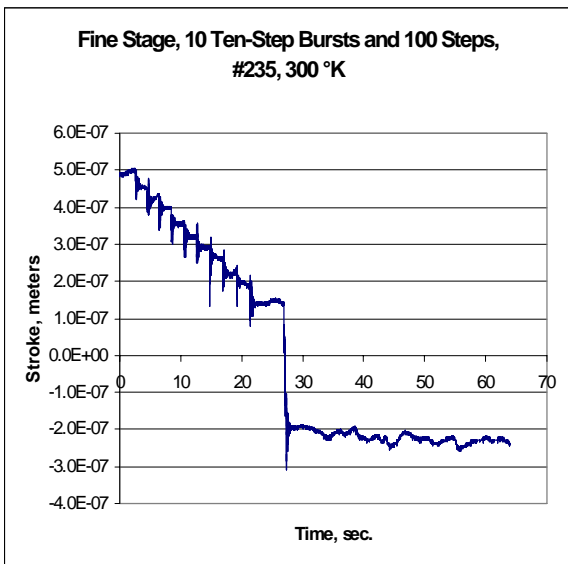


Figure 10. Fine stage, ten step increments

stage (equivalent to one motor step) is about 3.2 nanometers.

A detail of one of the steps may be seen in Figure 11. The apparent change in position is about 33 nanometers ($3.55\text{E-}07$ - $3.22\text{E-}07$ meters). One would expect 32.5 nanometers based upon the 100 motor step burst analyzed in the previous paragraph. The ten bursts are reasonably uniform and of similar displacement magnitude.

One may also observe a damped oscillation which takes about three-quarters of a second to be obscured by the ambient noise. The initial amplitude of the oscillation is about 90 nanometers peak-to-valley and has a period of about .25 seconds (frequency of 4 Hz.). The noise appears to be about 10 to 15 nanometers peak-to-valley. The damped oscillation occurs when the motion of the actuator disturbs the equilibrium position of the rods that support the test fixture, getting them to vibrate. The noise is generated by vibrations that are continuously excited by local environmental factors (acoustic and seismic).

3.5.2 The Response to Ten Bursts of Three Motor Steps Followed by One Burst of 100 Motor Steps

Figure 12 shows the response at room temperature of the actuator to test bursts of three motor steps. The interpretation of these data is a little more difficult than for the ten motor step burst discussed above. The movement caused by the 100 motor step burst may be between about 280 nanometers and about 400 nanometer depending upon how the local transient in the background is treated. The effect of a single motor step (resolution) would be between 2.8 nanometers and 4.0 nanometers with an average value of 3.4 nanometers. In this case the ten bursts are of considerably different displacement magnitude.

Figure 13 is a detail of one burst of motor steps from Figure 12. The apparent change in position is between about 18 nanometers and about 25 nanometers depending upon the treatment of the local transient in the background. From Figure 12 it may be observed that the effect of the three motor step bursts appears to vary between 0.0 nanometers and perhaps as

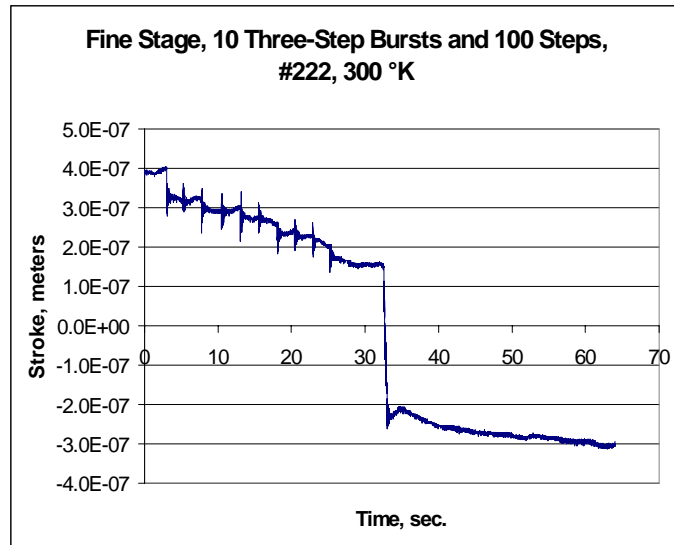


Figure 12. Fine stage, three step increments.

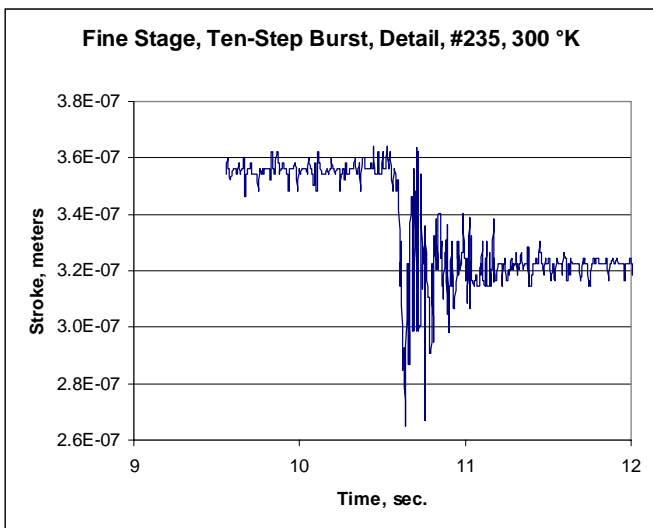


Figure 11. Detail of a ten step increment.

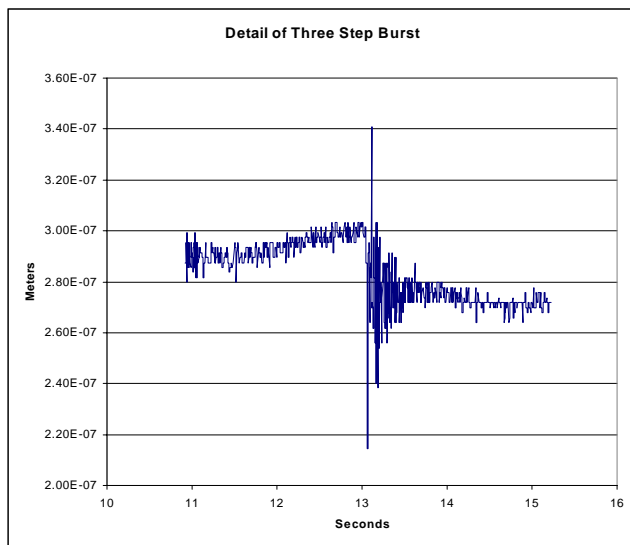


Figure 13. Detail of a three step increment.

much as 80 nanometers. One would expect about 102 nanometers from the average value of the 100-burst motion. The net effect of the ten bursts of three motor steps is about 160 nanometers after removal of the drift shown at the end of the data (after about 32 seconds in Figure 12); in poor agreement with 102 nanometers based upon the 100 motor step burst.

The initial amplitude of the damped oscillatory response (in Figure 13) is about 125 nanometers peak-to-valley and the background noise is between 10 and 20 nanometers peak-to-valley, similar to the observed values in the detail of the ten motor step burst. The magnitude of the local transient effect is quite large (compare Figure 13 to Figure 11). In general, the combined effects of the noise, drift and local transients make it very difficult to compare the sizes of the ten increments in Figure 12. The rapid changes during quiescent periods suggest an environmental effect which may be parasitic to the actuator operation or part of the operating background. Among repeated runs of this test sequence some appeared to be better and some were worse. A consistent pattern was difficult to discern.

3.5.3 Response to Ten Bursts of One Motor Step Followed by One Burst of 100 Motor Steps

Figure 14 shows the response (at 20° K) of the actuator to ten bursts of single motor steps followed by one burst of 100 motor steps. The response to the 100 motor step burst is about 310 nanometers for a one-step resolution of about 3.1 nanometers per motor step, somewhat lower than the previously analyzed 100 motor step bursts (which were at 300° K). The difference cannot be due to the low temperature since most of the other measurements at cold temperature confirm the 3.2 to 3.3 nanometer motor step effect (resolution).

The net effect of the ten bursts of single motor steps is about 30 to 35 nanometers. This is about what is expected from the 100 motor step burst, however the individual increments are uneven and some appear to be the reverse of the expected direction (retracting). The overall drift is very small so the variation cannot be blamed on this.

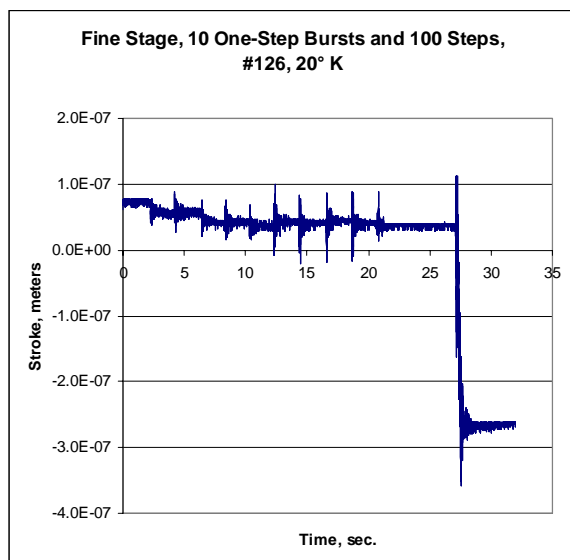


Figure 14. Fine stage, single step increments

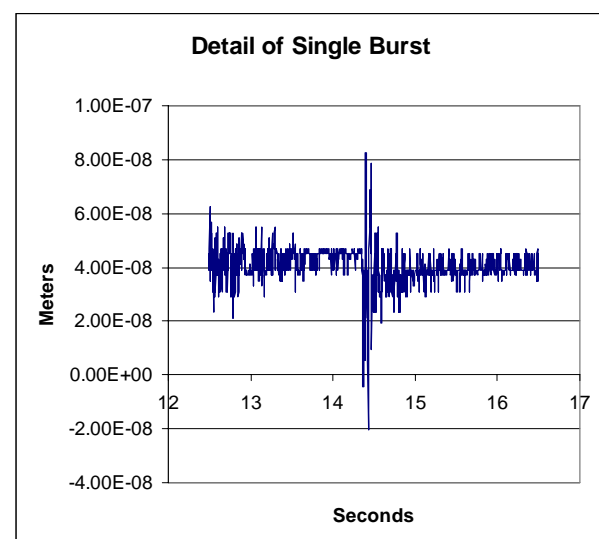


Figure 15. Detail of a single step increment

Figure 15 shows a detail of one burst in Figure 14. The initial amplitude of the oscillation is about 100 nanometers peak-to-valley and the noise is about 10 nanometers peak-to-valley, similar to the room temperature values. The increment of motion appears to be 0.0 nanometers.

3.6 Testing Cryogenic Heat Dissipation

Figure 16 shows the results of calorimetric heat dissipation tests performed on the fine stage at a temperature of about 20°

K. In test number 147 the fine stage was cycled through its full stroke, 9,000 motor steps extending followed by 9,000 motor steps retracting. This test took about 125 seconds and resulted in a temperature rise on the fine stage motor housing of about 2.55 K° . The test had been run at a motor current of .400 amperes. The same test was rerun, test 148, without commutating the current through the windings, thereby leaving the motor stationary (not turning). The result was a temperature rise of only $.57\text{ K}^{\circ}$.

In an attempt to simulate the heating effect of test 147 the current was increased to .75 amperes and the non-commutat-

ing test rerun, test 149. The result was a temperature rise of about 3.15 K° , slightly larger than that of test 147 where the stage had been cycled through its full stroke. Although the temperature rise in test 149 was slightly greater than in test 147 the peak is narrower (see the figure) giving the impression that the net heating was about the same. The resistance of the windings at this temperature had been measured at .50 ohms. The instantaneous power required to drive the fine stage at 20 K° is then,

$$\text{power} = 2 \times (.75/2)^2 \times .5 = .14 \text{ watts.}$$

Note that in the calculation the current is divided between two windings (resistances in parallel).

3.7 Discussion of the Test Data From JPL.

The data from the tests at JPL were largely consistent with the expected behavior of the actuator based upon analysis of its mechanics. The JPL data for the larger motions (over about .1 micrometer) were quite accurate and repeatable at both room temperature and cryogenic temperature. The data for smaller motions became difficult to interpret as one approached the resolution of the interferometer, about 7 nanometers.

3.7.1 The Stroke of the Coarse Stage.

The stroke of the coarse stage was demonstrated to be greater than about 10.1 millimeters at both room temperature and cryogenic temperature. A reduced stroke at low temperature due to thermal contraction of the metals of construction between 300 K and 20 K would be about .2% but the data are not able to resolve it.

3.7.2 The Stroke of the Fine Stage.

The demonstrated stroke of the fine stage was 25.98 micrometers for the 8000 motor steps or about 3.2 nanometers per motor step. The fine stage design had anticipated a nominal value of 2.7 nanometers per motor step. The difference is probably due to the coil spring being stiffer than the nominal design.

3.7.3 The Smallest Increment in the Coarse Stage.

The measurements of the smallest increments for the coarse stage showed an average size of about .58 micrometers with a variation of .074 micrometers rms. The stage has 1085 motor steps per revolution of the lead nut. The thread between the lead nut and the screw is a standard .112-40UNC thread form that should advance the screw by .585 micrometers for each

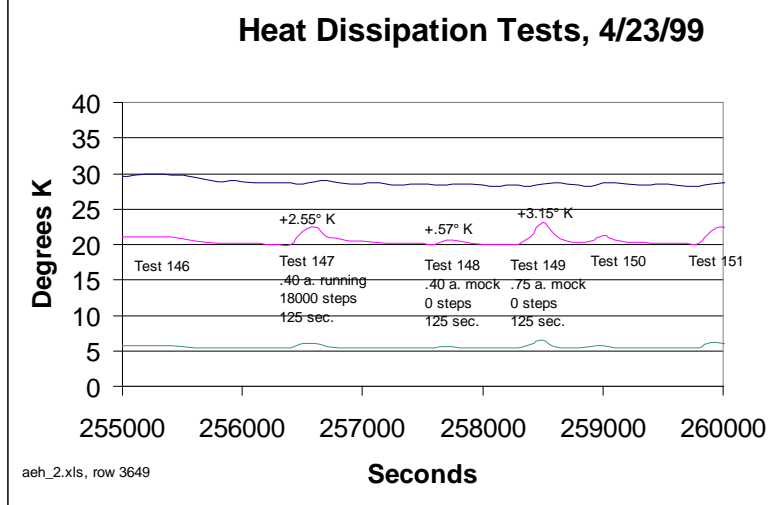


Figure 16. Calorimetric heating tests at 20 K° .

motor step. The smallest increment in the coarse stage is therefore represented by a single motor step.

The variation in the step sizes of .074 micrometers is about at the limit of consistency for a well-made and matched screw thread and nut.

3.7.4 The Smallest Increment in the Fine Stage.

The smallest motion increment in the fine stage appears to be between 1 and 10 motor steps at both room temperature and cryogenic temperature. Tests of the smaller increment sizes (one and three steps each) were strongly influenced by other factors; noise, oscillations, drifts. Although it appeared that the actuator was behaving about right, actual observation of the actuator's behavior was obscured by these other influences, some of which could be generated by the actuator.

3.7.5 Cryogenic Power Requirements and Heat Dissipation in Calibration Mode

From the calorimetric comparisons discussed in section 3.5.4 the heat dissipated in the fine stage of the actuator was shown to be

power = .14 watts

during cryogenic operation.

Assuming the actuator is run at 200 steps per second the energy required per motor step is,

energy per step = .14/200 = .0007 joules.

If the calibration period is two hours (7200 seconds) and requires 1200 motor steps from the actuator (800 coarse and 400 fine)) the average heat dissipation during Calibration Mode is,

Heat Dissipation, CM = .0007 x 1200/7200 = .117 milliwatts

at 20° K.

The requirement for NGST is to be less than 5.0 milliwatts and the goal is to be less than 0.5 milliwatt. The measured performance is less than both by good margins.

Assuming that the controller operates at high efficiency (which is consistent with observations made during the tests) all of the electrical power will show up as heat dissipation and they will be equal. Therefore the average power required during Calibration Mode is,

Power Consumption, CM = .000117 watts.

The requirement for NGST is to be less than 1.0 watt and the goal is to be less than 0.1 watts. The measured performance of the actuator is smaller than both of these by large factors.

3.7.6 Power and Heating in Observatory Mode

Between all tests and over the full temperature range the electrical power was completely removed from the Rubicon actuator. The actuator held its set position without perceptible drift or wandering which might require active repositioning of the device. Therefore,

OM Heat Dissipation and OM Power Consumption = 0.0 watts.

4.0 The Test Program at Moog-SMD

Before testing was begun at SMD both the actuator and the controller designs were reviewed and modified. Control of the motors' current was improved by incorporating a "pulse width control" circuit which reduced parasitic heating in the motor windings. The fine stage of the actuator was modified to reduce the backlash and friction effects in the Rubicon transducer. The coil spring in the Rubicon transducer was also replaced by a new spring which was about 20% stiffer, increasing the resolution of the fine stage to about 4 nanometers per motor step.

The actuator was installed in the capacitance metrology facility established at SMD to study in some detail the smallest motion increments of the fine stage. Figure 17 is a photograph of the test article showing the fine stage and thrust rod on the right and the coarse stage motor on the left. The Rubicon transducer is in the slotted portion between them. It is shown about actual size.

Capacitance gauge metrology is strongly affected by electromagnetic interference in the vicinity of the test setup. Several locations at SMD were evaluated and a location with reasonably low noise was selected. Figure 18 shows a 40 second sample of the background noise (converted to equivalent displacement error) with the actuator powered off. The recorded noise level was about 1.18 nanometers, rms.



Figure 17. The Rubicon actuator, about actual size.

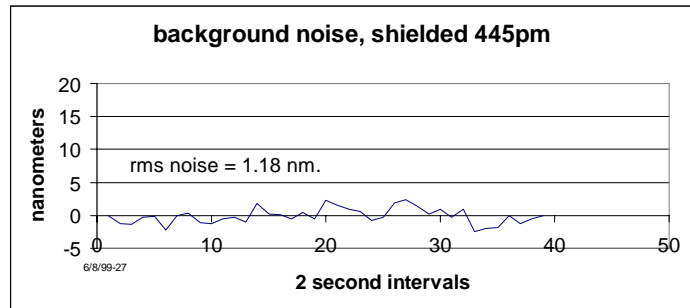


Figure 18. Typical background noise at SMD.

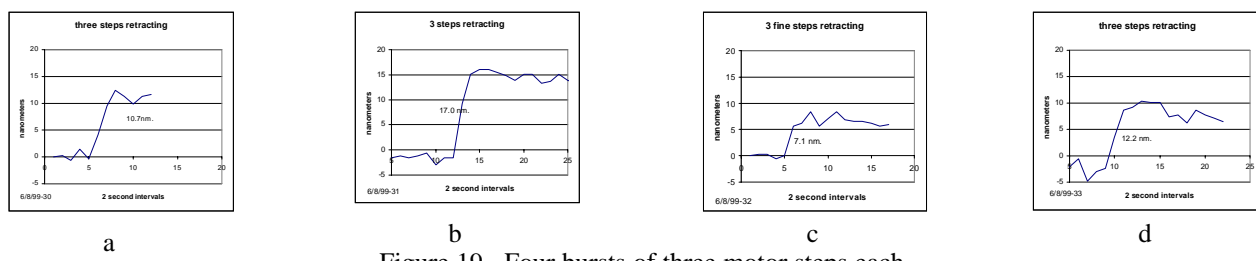


Figure 19. Four bursts of three motor steps each.

To determine the influence of the noise on our ability to measure the actuator's behavior we measured four identical bursts of three motor steps each. Each of the bursts was recorded separately and several minutes passed before the next burst was performed and measured. The four bursts are shown in Figures 19a, b, c and d. Each of the three step bursts was clearly distinguishable from the background noise which appears not to have changed and the height of each burst is indicated on its Figure. The statistics for these data are,

mean burst motion:	11.75 nm.
std. deviation of bursts:	3.55 nm.
mean motor step:	3.92 nm.

The increased size of the mean motor step, 3.9 nm. compared to 3.2 nm. at JPL, was due to changing the coil spring to a slightly (~20%) stiffer configuration. Since the standard deviation of the burst motions was considerably larger than the background noise we were now confident that we were observing actuator behavior and continued with our tests.

4.1 Testing the Smallest Increment of the Fine Stage

Figure 20 shows a plot of ten sequential bursts of ten motor steps each. The average height of the bursts is 38.6 nanometers with a variation of 4.0 nanometers, rms., about one motor step. (Note the increased effect of a motor step caused by the increased stiffness of the new spring.)

Figure 21 shows a plot of ten bursts of two motor steps each. The average burst height is 7.9 nanometers and the variation is 2.21 nanometers, rms., somewhat less than a single motor step.

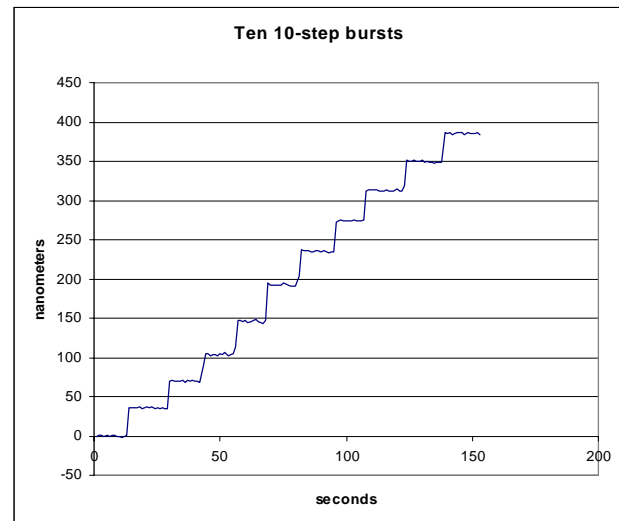


Figure 20. Fine stage, ten step increments.

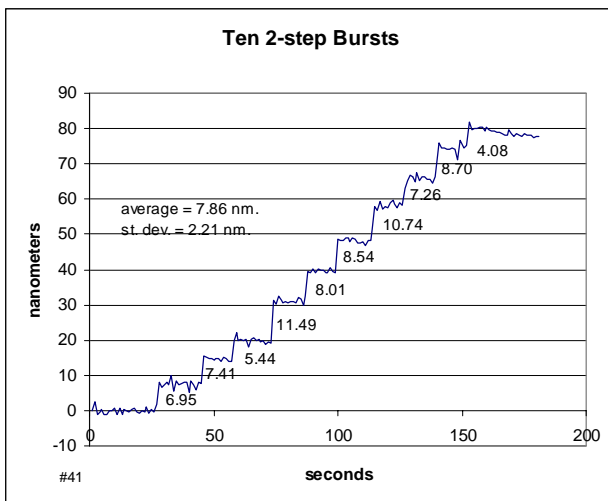


Figure 21. Fine stage, two step increments.

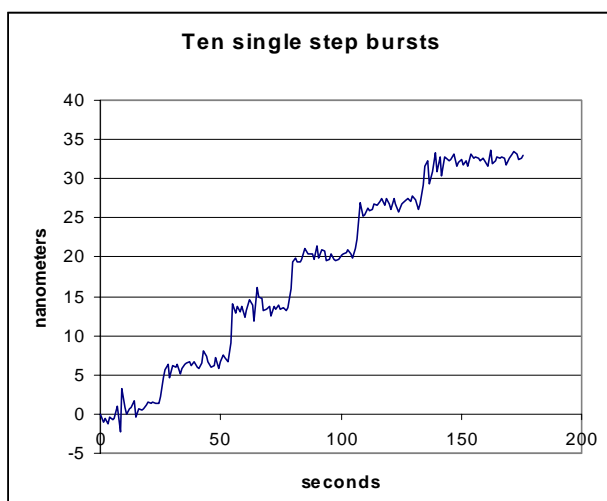


Figure 22. Fine stage, single step increments.

Figure 22 shows a plot of ten bursts of one motor step each. In this case it appears that the Rubicon transducer was not able to convert each individual motor step into a corresponding actuator motion. The net motion for all ten bursts was about 33. nanometers. The actuator did not respond directly to each of the motor steps that was commanded.

4.2 Testing the Room Temperature Power Consumption

The power required to operate the fine stage of the actuator was determined by measuring the DC current from the power supply and measuring the average voltage that was driving the current:

DC current: .350 amperes
average voltage: 9.5 volts

The product of these is the instantaneous electrical power required to drive the actuator fine stage at room temperature,

power = .35 x 9.5 = 3.3 watts.

4.3 Testing the Mass of the Actuator

The Rubicon actuator was first assembled with a long (72 inches) electrical cable attached to it which greatly facilitated testing at both JPL and SMD. In this configuration the mass was measured to be 273 grams. The excess cable was estimated to be about 40 grams, so the actuator's mass was estimated to be between 230 grams and 235 grams.

Prior to delivery the electrical cable was trimmed to agree with the Interface Control Drawing (see Appendix B), 3.0 inches in length and the mass was re-measured,

actuator mass = 243 grams

4.4 Discussion of the Test Data from SMD.

4.4.1 The Smallest Increment of Motion in the Fine Stage of the Actuator

The low noise and high resolving power of the facility at SMD allowed the detail study of the fine stage of the Rubicon actuator. A summary of the data appear in the following table with a comparison of the mean of the motor step sizes:

Motor Steps in Each Burst	Number of Bursts	Mean of Burst Motions	Mean Motor Step Size	Std. Dev.
10	10	38.6	3.86	4.0
3	4	11.75	3.92	3.55
2	10	7.9	3.95	2.21
1	10	3.2	3.2	4.5
			3.73 mean	3.56 mean

From these data it may be observed that the uncertainty in the motion of the fine stage is equivalent to about one motor step and is independent of the number of motor steps commanded in each burst. Furthermore, individual motor steps are not reliably produced in the output motion. Therefore, the smallest increment of motion that may be produced in the output is equivalent to two motor steps, or 7.9 nanometers in the configuration using the stiffer coil spring.

All the tests at SMD were performed at room temperature. The tests at JPL demonstrated no observable or measurable differences in the response of the actuator between room temperature and cryogenic temperature. Consequently, it is expected that the smallest increment at cryogenic temperature will also be 7.9 nanometers with a variation of about 3.56 nanometers, rms.

4.4.2 Room Temperature Power Requirements and Heat Dissipation in Calibration Mode.

The room temperature power required for the fine stage of the actuator was measured to be

power = 3.3 watts.

Assuming that the actuator is run at 200 steps per second the energy required per motor step is,

energy per step = $3.3/200 = .0165$ joules.

If the calibration period is two hours long (7200 seconds) and requires 1200 motor steps from the actuator (800 coarse and 400 fine) the average power during Calibration Mode is,

Power Consumption, CM = .0165 x 1200/7200 = .00275 watts

at room temperature. The requirement for NGST is to be less than 1.0 watt and the goal is to be less than 0.1 watt. The measured performance exceeds both by a sizeable margin.

The controller for the motor uses a very small fraction of the power supplied to the actuator so that one may assume that most of the electrical power will be dissipated in the actuator as electrical losses or frictional heating. For purposes of analysis the heat dissipation is assumed to be equal to the electrical power so that the average heat dissipation in Calibration Mode is,

Heat Dissipation, CM = 2.75 milliwatts.

The requirement for NGST is to be less than 5.0 milliwatts and the goal is to be less than 0.5 milliwatts. The measured performance is less than the requirement by a factor of 1.8 but does not meet the goal for the assumed calibration cycle.

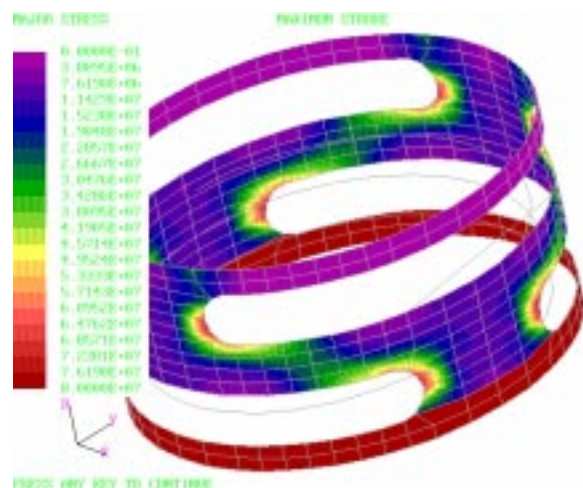


Figure 23. A finite element analysis of the transducer.

5.0 Analysis of the Other Properties

5.1 Elastic Properties of the Rubicon Fine Transducer

Analysis of the actuator's properties begins with a finite element analysis to determine the elastic properties of the fine transducer. One model used in the analysis of this actuator is shown in Figure 23. The dominant feature in the figure is the model of the slotted cylindrical shell but included in the model is the coil spring which controls the state of strain in the cylindrical shell. In the figure the bottom end of the coil spring is attached to the bottom edge of the slotted cylinder with rigid elements. The top end of the coil spring is free while the top end of the slotted cylinder is rigidly fixed. The finite element model is loaded by displacing the free end of the coil spring through a fixed axial distance, 6.5 millimeters in this case (equivalent to about ten turns of the lead screw inside the nut of the pressure plate). Several such models were made to determine the appropriate proportions of the slotted cylinder. The proportions of the NGST actuator found the following responses to the 6.5 millimeters displacement:

Axial load on the pressure plate, nut and lead screw = 39.2 N

Change in length of the slotted cylinder = .0302 mm.

Major stress in shell = 119.6 MPa. = 17,460 psi.

Shear stress in coil spring = 171 MPa. = 24,900 psi.

Axial stiffness of shell = 1.3×10^6 N/m

Effectiveness Ratio = transducer input/transducer output = $6.5/.0302 = 1:00462$

The coil spring is wound from 302 stainless steel with a tensile strength of 232,000 to 262,000 psi tensile strength. The slotted cylinder is machined from 416 stainless steel in the as-fabricated condition with a tensile strength of about 70,000 psi. (it has not been heat treated for strength). The maximum stresses in both components are small compared to strengths of their materials.

5.2 Analysis of Creep

Available data for stainless steels (Marshall and Maringer, 1977) suggest there is a threshold stress of about 14,000 psi. below which no creep occurs at room temperature. Furthermore, this threshold rises as the temperature is reduced. At room temperature and 17,500 psi. tensile stress the creep rate is about 100 parts per million in 500 hours (4.8 ppm/day).

Only the portions of the transducer which see stresses above about 14,000 psi. will experience any creep at all and the average creep over this portion of the transducer will be half the maximum, 2.4 ppm/day. If the stresses which may give rise to creep are assumed to occupy about 5% the shell structure, a conservative assumption which may be verified by reference to Figure 23, then the net creep in the transducer at maximum stroke may be bounded as,

$$\text{creep} < .05 \times 2.4 \times 10^{-6} \times 30.2 \times 10^{-6} = 3.62 \times 10^{-12} \text{ meters per day} = .00362 \text{ nanometers/day at room temperature.}$$

This provides an upper bound for the creep at room temperature and maximum transducer extension. Over most of the useful range of motion of the transducer (when maximum stresses are below 14,000 psi.) there will be no creep at all. Also, at temperatures below about 200° K there will be no creep even at the highest stress levels.

5.3 Analysis of Loads Between the Lead Screws and Nuts

The properties of the coarse and fine lead screws and nuts are presented in the following table:

Parameter	Coarse Stage	Fine Stage
Lead Screw	Translating	Rotating
Nut	Rotating	Translating
Thread*	.112-40UNC-2A/B	.219-40UNS-2A/B
Form*	Unified National	Unified Special
Maximum Axial Force, N	8.0	39.2
Minimum Axial Force, N	6.0	~0.0
Average Axial Force, N	7.0	19.6
Threads Engaged	6	6
Ave. Contact Area, 10-6 m ²	11.52	25.2
Ave. Contact Pressure, MPa	.521	.766
Coefficient of Friction	.25	.25
Max. Friction Torque, N-m	.0043	.033

*Handbook H28, U. S. Dept. of Commerce

In the coarse stage the axial forces are generated by a combination of both the external axial force (assumed here to be 4.0 N) and a spring preload which varies from 2.0 N to 4.0 N depending upon the position of the output thrust rod. The axial preload is applied to assure that for small loads on the actuator the lead screw and nut will always be contacting on the same flank of the thread form.

The contact pressures are low, about 100 psi. or less, assuming only six threads are in contact. The coefficient of friction is also high for tungsten disulfide (Dichronite) which has a normal value of about .05, five times lower than that used in the analysis. Consequently, the friction torques shown at the bottom of the table above are reasonably conservative. The maximum friction torque on the fine stage lead screw is almost an order of magnitude larger than that on the coarse stage nut (note that the lead screw/nut combination is inverted between the two stages).

5.4 Lifecycles

Assuming a typical operational cycle of the actuator is 800 coarse motor steps and 400 fine motor steps and the average contact pressures calculated above, the expected number of such operating cycles may be calculated as shown in the table below:

Parameter		Coarse Stage	Fine Stage
Average Contact Pressure, MPa	.	521	.766
Materials:			
Screw		440C	440C
Nut		Nitronic 60	Nitronic 60
Pitch Dia., in. ,mm.		0.09625 2.44	.2002 5.09
Pitch Diameter Travel per Cycle, mm.		5.67	5.89
Estimated Wear Rate, /MPa		1.2×10^{-10}	1.2×10^{-10}
Allowable Wear, m		$.5 \times 10^{-6}$	$.5 \times 10^{-6}$
Total Sliding Distance, m		8,000	5,400
Limit of Operational Cycles, 10^6 cycles		1.41	.92

The estimated wear rate is a reasonably conservative value selected from the published literature for the wear of dry lubricants in vacuum. The allowable wear is the nominal single thickness of the tungsten disulfide dry lubricant as normally applied (two surfaces in contact have a double thickness of the dry lubricant at their interface). The total sliding distance is equal to the allowable wear divided by the estimated wear rate and the average contact pressure. Finally, the limit of the number of operational cycles that meets the criterion for allowable wear is the total sliding distance divided by the pitch diameter travel per cycle.

In practice the number of operational cycles to expect from the actuator will depend somewhat upon the way the actuator is actually operated and the degree of similarity between the actuator's mechanisms and the test machines from which estimated wear rate data were taken. Individuals may wish to adjust the above estimates based upon the service conditions they expect in their applications.

5.5 Analysis of the Motor Size

The friction torque at the fine stage lead screw has been estimated to be .033 N-m. (see 5.3 above). The coarse stage friction torque is much lower. The reducing gearhead has a ratio of 45.2:1 and an estimated efficiency of 88% so the torque load at the fine stage motor shaft is

$$\text{torque load at motor shaft} = .033/(45.2 \times .88) = .000830 \text{ N-m.}$$

Good motor design practice requires a factor of three on the anticipated maximum load so that the torque required of the motor at its shaft is

$$\text{motor shaft torque} = .000830 \times 3 = .00249 \text{ N-m.}$$

The stepper motor used in the actuator has a holding torque capability between .05 and .07 N-m. which is twenty to thirty times larger than the required output from the motor. The motor chosen for this design was the smallest motor on which Moog-SMD had existing engineering data and a proven flight history and there were insufficient resources on the project to develop a new qualifiable motor design. The motor provides generous safe margin for operating the actuator but also accounts for most of the mass. Because of its large size it is operating very inefficiently (at room temperature, particularly) and accounts for most of the room temperature power and heat dissipation.

5.6 Analysis of the Axial Stiffness

The axial stiffness of the actuator is net effect of the stiffness of several components of the actuator, all in series:

$$K_{\text{Thrust Rod}} = 9.4 \times 10^6 \text{ N/m.}$$

$$K_{\text{Bearing}} = 8.2 \times 10^6 \text{ N/m.}$$

$$K_{\text{Bearing Plate}} = 250. \times 10^6 \text{ N/m.}$$

$$K_{\text{Transducer}} = 1.3 \times 10^6 \text{ N/m.}$$

$$K_{\text{Motor Housing}} = 390. \times 10^6 \text{ N/m.}$$

$$K_{\text{net}} = 1.00 \times 10^6 \text{ N/m.}$$

The net axial stiffness is dominated by the stiffness of the cylindrical shell of the fine transducer, it being much the softest of all the components that are in series. Changes to the stiffness of the actuator are effected most easily by changing the stiffness of the transducer shell.

5.7 Analysis of Axial Force, Set & Hold

The actuator can hold a set position under any force up to the strength of the weakest of its component parts. In the design that has been tested those weakest components are the thrust bearing which supports the thrust rod in the coarse stage and the slotted cylinder of the fine transducer. The fine transducer is currently limited to about 120 Newtons axial load but with heat treatment its strength could be increased by a factor of two or three. The thrust bearing supporting the thrust rod currently has a static capacity limit of about 130 Newtons and increasing this value will require larger bearings for supporting the thrust rod in the coarse stage. Operating at these high loads may cause an increase in the room temperature creep of the fine transducer.

5.8 Analysis of Thermal Stability

The Rubicon actuator for NGST is athermalized at mid-stroke, that is at 5.0 millimeters extension. Athermalization is accomplished by adjusting the material composition of the thrust rod. The thrust rod is about 68 millimeters long at mid-stroke and it is composed of 63.35 millimeters of 440C stainless steel and 4.64 millimeters of Invar. The Invar is at the output end of the thrust rod and is attached to the stainless steel portion with adhesive and a small dowel pin. Details of the athermalization calculation are shown in Appendix A.

As the thrust rod moves away from the mid-stroke position it acquires some thermal sensitivity from the increasing proportion of 440C stainless steel in the over all length (if the thrust rod is extending) or decreasing proportion (if retracting). At the fully extended limit the thermal sensitivity is about 50 nanometers/K and at the fully retracted position it is about -50 nanometers/K. These values are for room temperature properties of the materials. At 20° K the thermal expansion coefficients for most of the materials fall off by about a factor of 100 so the thermal sensitivity at these low temperatures is about ±.50 nanometers/K.

It may be possible to materially reduce the thermal sensitivity of the actuator by reversing the positions of Invar and 440C in the thrust rod. The materials of the nuts (Nitronic 60) and lead screws (440C) were selected for their resistance to abrasion, galling and wear in high vacuum environments. This is in case the dry film lubricant is lost or worn away during service. The calculation of the lifecycles suggests that the dry film itself may be sufficient to support the operation over the desired life. If the threaded portion of the lead screw is made from Invar (in stead of 440C) the thermal sensitivities at the limits of the stroke would be reduced by a factor of about 20, to ±2.5 nanometers/K at room temperature. Incorporating this into the design will first require some tribological testing to verify that Invar can serve suitably as the lead screw material.

6.0 An Analytical Model for Systems Simulations

An analytical model of the Rubicon actuator may be easily developed for any analytical software that solves linear equations. The actuator's mass is 243 grams and is nearly equally divided between the coarse and fine stages. The two stages are joined by the cylindrical shell of the fine transducer. The axial stiffness of the actuator is one million Newtons per meter, so the axial stiffness of the cylindrical shell may be represented by a spring of this stiffness. In a system simulation the mass representing the fine stage should be attached to the structural foundation. The spring representing the cylindrical shell should be attached to the mass of the fine stage and the mass representing the coarse stage should be mounted to the

opposite end of the spring representing the cylindrical shell. Motions and disturbances of the mass representing the coarse stage are superimposed on the output of the actuator so a stiff element (the thrust rod) should be returned from the mass of the coarse stage to the mounting point on the structural foundation. A schematic representation of this suggested model is shown in Figure 24.

7.0 Requirements Compliance Matrix

The Rubicon structural actuator has been tested at both room temperature and cryogenic temperature for compliance with the requirements and goals for the properties of NGST. Some properties which were unamenable to test were evaluated by analysis. The results of both are shown in the following table. The NGST requirements and goals have been included in the table for reference.

Property	NGST		Rubicon Performance at Temperature (°K)		Basis	Report Paragraph
	Requirement	Goal	20	300		
Resolution, smallest increment (nanometers)	£20	£10	7.9	7.9	Test	4.4.1
Lifecycles	³ 10,000	³ 1,000,000	920,000	920,000	Analysis	5.4
Stroke (millimeters)	³ 6	³ 10	10.1	10.1	Test	3.7.1
Operating temperature (Kelvin)	20-60	20-300	20	300	Test	3.0
CM Heat Dissipation (milliwatts)	£5	£0.5	.151	2.8	Test	3.7.5/4.4.2
OM Heat Dissipation (milliwatts)	£0.05	0	0.0	0.0	Test	3.7.6
Mass (grams)	£40	£20	243	243	Test	4.3
Outside Diameter (centimeters)	£5	£1	4.05	4.05	Test	8.0
Creep, OM (nanometers/day)	£0.1	£0.01	0.0	<.01	Analysis	5.2
Thermal Stability, OM (nanometers/Kelvin)	£50	£20	<.5	<50.	Analysis	5.8
Axial Force, set & hold, OM (N)	³ 0.5	³ 1	120	120	Analysis	5.7
Power Consumption, CM (watts)	£1	£0.1	.000151	.0028	Test	3.7.5/4.4.2
Axial Stiffness (N/micrometer)	³ 1	³ 1	1.0	1.0	Analysis	5.6
Stowed Axial Length (centimeters)	£10	£10	10.	10.	Test	8.0

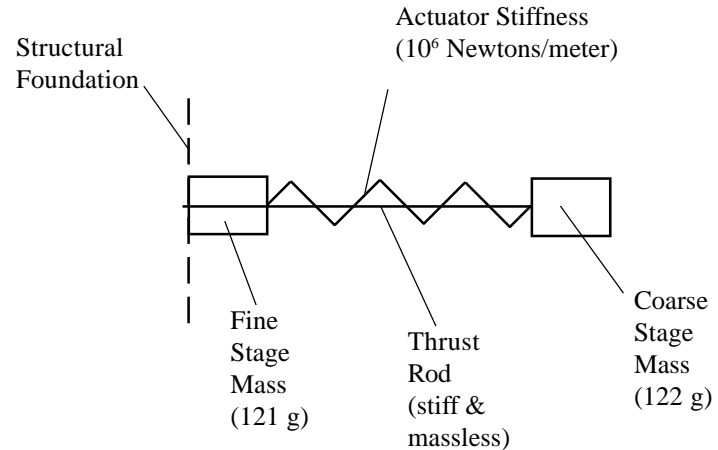


Figure 24. Schematic diagram of simulation model.

8.0 Installation Data

The Interface Control Drawing, AEH drawing 93600, is shown in Appendix B and includes as-built dimensions.

9.0 References

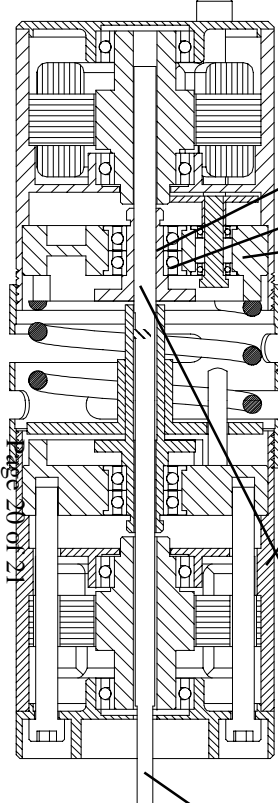
Hatheway, Alson E., "Metrology for Characterizing Actuators with sub-atomic Repeatability," *Proceedings of the Annual Meeting*, (Raleigh, NC, American Society of Precision Engineers, 1994), pp.246-9

Marschall, Charles W. and Maringer, Robert E., *Dimensional Instability*, (New York, Pergamon Press, 1977), p. 125

"Rubicon" is a trademark of Alson E. Hatheway Inc. The Rubicon transducer is patented by Alson E. Hatheway Inc.
Page 19 of 21

Thermal Stability

Appendix A



Component	Mat.	CTE (ppm/K°)	Length (mm.)	CTE x Length (mm.-ppm/K°)
Coarse Lead Nut	Nit. 60	16.2	5.0	81.0
Bearing	440C	10.08	-0.5	-5.04
Gear Plate	Ti6Al4V	9.54	3.5	33.89
Rubicon Shell	416	9.9	20.	198.
Motor Housing	Ti6Al4V	9.54	35.	333.9
Total:			63.	641.25

At mid-stroke the thrust rod length will be $63. + 10/2 = 68.$ mm.
If length x is made of Invar, .566 ppm/K°, and the rest is made of 440C,

$$10.08(68 - x) + .566 x = 641.25; x = 4.64 \text{ mm.}$$

$$685.44 - 10.08x + .566x = 641.25$$

$$x = 44.19/9.51 = 4.64 \text{ mm.}$$

Thrust rod construction:
440C stainless, 63.35 mm.
Invar, 4.64 mm.

Thermal sensitivity = $\pm 5.0 \times 10^{-3} \times 10.08 \times 10^{-6} = 0.0 \text{ to } \pm 50. \text{ nm./K}^{\circ}$

Appendix B

